EPSC2017

SB10 abstracts

EPSC Abstracts
Vol. 11, EPSC2017-110, 2017
European Planetary Science Congress 2017

On the synergy of polarimetry and spectroscopy for the physical characterization of the asteroids

A. Cellino
(1) INAF, Osservatorio Astrofisico di Torino, Italy (cellino@oato.inaf.it / Fax: +39-011-8101930)

Abstract

The synergic use of polarimetry and visible/near-IR reflectance spectroscopy is a fundamental tool for the purposes of physical characterization of small solar system bodies, in particular the asteroids. A couple of major applications are asteroid taxonomy, and the study of the so-called Barbarian asteroids. In the field of taxonomy, a new identification of the F taxonomic class previously found in the 80s and then substantially lost due to a lack of spectroscopic data at short wavelengths is one of the expected results of the on-going Gaia mission. As for Barbarians, there are indications that they might be extremely old and primitive.

1. Introduction

Reflectance spectroscopy is one of the most intensively adopted technique to obtain data of utmost importance for the purposes of asteroid physical characterization. Reflectance spectra are extensively used to infer information about the most likely composition of asteroid surfaces and are also the basis of asteroid taxonomy. Polarimetry has been known since a long time to be a primary tool for the determination of the geometric albedo and of the sizes of surface regolith particles, but due to the fact of requiring several observations of any single object, observed at different phase angles, polarimetry has been strongly under-exploited for a long time. The recent availability of new observing facilities and the beginning of new dedicated observing campaigns, like the *Calern Asteroid Polarimetric Survey* (CAPS), in addition to a first systematic project of spectro-polarimetric observations has started to change the situation. Two fields in which the synergy of polarimetry and reflectance spectroscopy is particularly promising are asteroid taxonomy and the study of the so-called Barbarian asteroids.

2. Asteroid taxonomy: the recovery of the F class

Polarimetric data were used in the first era of asteroid taxonomic classification to distinguish among objects having nearly identical UBVRI colours, but very different albedo. Subsequently, taxonomy started to be based on full reflectance spectra obtained in the framework of extensive campaigns like the SMASS [1], while the data-set of asteroid polarimetric data became fully insufficient to be used as a support to taxonomic classification. Modern asteroid spectroscopy has covered mostly the visible and near-IR spectral region, while the blue part of the spectrum has been essentially lost. As a consequence, the previously identified F class [2] has been no longer recognized in modern taxonomies, and the objects previously found to belong to the F class are now included in a bigger class named B. However, polarimetric data in V colour clearly show that F class asteroids are clearly distinct, being characterized by low values of the inversion angle of polarization, as shown in Fig. 1. Interestingly, some asteroids previously classified as F have been subsequently found to exhibit some cometary activity, like in the case of (4015) Wilson Harrington, and of (3200) Phaethon, the likely parent body of the Geminids meteor shower. This makes F-class asteroids particularly interesting. One of the expected results of the ongoing Gaia mission will be that of being able to identify F class asteroids taking profit of the fact of performing spectroscopy over a wavelength range including the blue. Ground-based polarimetric data will be essential to confirm and validate Gaia results in this field.

3. Barbarians

Barbarian asteroids, so called after the prototype of the class, asteroid (234) Barbara, are characterized by unusually large values of the polarization inversion angle (the phase-polarization curve of (234) Bar-

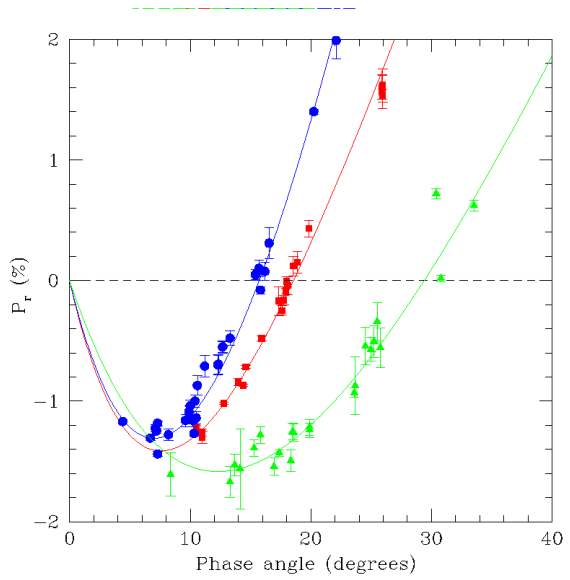

Figure 1: Phase-polarization curves of (704) Interamnia (F class, blue circles), (2) Pallas (B class, red squares) and (234) Barbara (Barbarian, green triangles). The best-fit curves corresponding to an exponential-linear function are also shown for each object.

bara is shown in Fig. 1). This property, first found by [3], is now shared by about 20 asteroids, most of which are fairly big in size (> 50 km). Barbarians are now known to be characterized by peculiar reflectance spectra, interpreted in terms of an anomalous composition rich in spinel, a refractory mineral found in Calcium-Aluminum-rich inclusions (CAIs) in many meteorites. CAIs are considered to be the oldest samples of solid material found in the solar system [4]. The Barbarian properties are not due to a thin surface layer, but they are structural, as indicated by the discovery of a family of Barbarian asteroids [5]. Barbarians could therefore potentially represent the Holy Graal in asteroid studies, namely survivors of the first generation of planetesimals accreted in the inner solar system. For this reason, spectro-polarimetric studies of these objects are being actively carried out by different teams.

4. Summary and Conclusions

The synergy of polarimetry and spectroscopy is reveling new and exciting fields of investigation in the field of asteroid science. In addition to the use of separate polarimetric and spectroscopic data, the simultaneous application of polarimetry and spectroscopy, made possible by the spectro-polarimetric observing mode offered at the ESO-VLT and at the WHT telescope, has been recently tested and preliminarily found to provide very interesting results ([6]). The reduction and analysis of a much larger data-set of measurements more recently obtained is currently under way, and a paper is in preparation.

Acknowledgements

This study would have not been possible without the help and collaboration of many colleagues. Among them, I mention S. Bagnulo, M. Devogele, P. Tanga, J. Sunshine, Ph. Bendjoya, E.F. Tedesco, I.N. Belskaya, J.-P. Rivet, G. Borisov, K. Muinonen.

References

[1] Bus, S.J., and Binzel, R.P.: Phase II of the Small Main-belt Asteroid Spectroscopic Survey, Icarus, Vol. 158, pp. 146-177, 2002.

[2] Gradie, J. and Tedesco, E.F.: Compositional structure of the asteroid belt, Science, Vol. 216, pp. 1405-1407, 1982.

[3] Cellino, A., Belskaya, I.N., Bendjoya, Ph., Di Martino, M., Gil-Hutton, R., Muinonen, K., and Tedesco, E.F.: The strange polarimetric behaviour of asteroid (234) Barbara, Icarus, Vol. 180, pp. 565-567, 2006.

[4] Sunshine, J.M., Connolly, H.C., McCoy, T.J., Bus, S.J., and La Croix, L.M.: Ancient asteroids enriched in refractory inclusions, Science, Vol. 320, pp.514-517, 2008.

[5] Cellino, A., Bagnulo, S., Tanga, P., Novaković, B., and Delbo, M.: A successful search of hidden Barbarians in the Watsonia asteroid family, MNRAS Letters, vol. 439, pp. L75-L79, 2014.

[6] Bagnulo, S., Cellino, A., and Sterzik, M.F.: Linear spectropolarimetry: a new diagnostic tool for the classification and characterization of asteroids, MNRAS Letters, Vol. 446, pp. L11-L15, 2015.

EPSC Abstracts
Vol. 11, EPSC2017-325, 2017
European Planetary Science Congress 2017

Spectro-polarimetry as a tool for characterizing small cosmic dust grains

O. Muñoz, F. Moreno, J. Escobar-Cerezo, and D. Guirado .
Instituto de Astrofísica de Andalucía, CSIC, Granada 18008, Spain (olga@iaa.es / Phone: +34 958 230609)

Abstract

In this work we show how experimental data of intensity and polarization of the scattered light of different cosmic dust analogues can be used to shed some light on the nature of dust particles. The experimental data are performed at various wavelengths (447, 520 and 647 nm) covering the scattering angle range from 3 to 177 degrees.

1. Introduction

Small dust particles are present in different scenarios in the Solar system like in the atmospheres of planets, satellites, and comets. Those particles can modify the temperature profile, dynamics, and chemical composition of the corresponding atmosphere. By analyzing the solar light scattered by those particles we can retrieve valuable information about their physical properties (shape, size, and composition). However, the quantification of the influence of dust particles in the atmosphere is far from trivial. Apart from its variable distribution in time and location, they usually present very irregular shapes. This introduces a serious difficulty in the radiative transfer modeling. While the treatment of the scattering processes from spherical dust particles is straightforward using Lorenz-Mie theory, it becomes much more complicated, or even impossible, for realistic poly-dispersions of irregular dust particles. Therefore, measurements of the full scattering matrices (including polarization) of realistic poly-dispersions of dust particles in the laboratory remain an extremely valuable tool for interpreting astronomical observations.

2. Experimental Apparatus

The scattering matrices of our samples are measured at the IAA COsmic DUst LABoratory (CODULAB) located at the Instituto de Astrofísica de Andalucía, Granada, Spain. For a detailed description of the experimental apparatus, calibration process, and data acquisition we refer to [Muñoz et al. (2010)]. Briefly, we use an Argon-Krypton laser as light source that can emits at three different wavelengths, 488, 520, and 647 nm. The laser beam passes through a polarizer and an electro-optic modulator. The modulated light is subsequently scattered by an ensemble of randomly oriented dust particles located in a jet stream produced by an aerosol generator. The scattered light passes through a quarter-wave plate and an analyzer (both optional) and is detected by a photomultiplier tube which moves along a ring. In this way a range of scattering angles from 3° to 177° is covered in the measurements. Another photomultiplier tube located at a fixed position is used to correct from fluctuations of the signal. We employ polarization modulation in combination with lock-in detection to obtain the entire four-by-four scattering matrix up to a constant. All matrix elements (except F_{11} itself) are normalized to F_{11}, that is, we consider F_{ij}/F_{11}, with i, j=1 to 4 with the exception of $i = j$ =1. The values of $F_{11}(\theta)$ are normalized so that they are equal to 1 at θ=30°. The function $F_{11}(\theta)$, normalized in this way, is called the phase function or scattering function in this work. The reliability of the apparatus has been tested by comparing measured scattering matrices of spherical water droplets at 488 nm, 520 nm and 647 nm with Lorenz-Mie computations [Muñoz et al. (2010)]. In addition, special tests have been performed to ensure that our experiment is performed under the single scattering regime [Muñoz et al. (2011)].

3. Measurements

The experimental data can be used in a direct manner, e.g. by comparison with astronomical observations of light scattered in single scattering conditions. An interesting example is related to cometary dust. As is observed in various comets the spectral dependence of the degree of linear polarization might be an indication of the composition of the sample under study [Mishchencko et al. (2010)]. In Figure 1, we present the measured degree of linear polarization

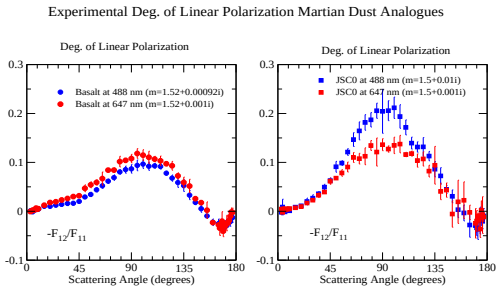

Figure 1: Measured degree of linear polarization for a Basalt sample (left panel) and JSC Mars-1 simulant (right panel).

Table 1: Estimated refractive indices ($m = n + ik$) of our Basalt and JSC Mars-1 samples [Pollack et al (1973)], [Clancy et al (1995)].

Sample	m(488 nm)	m(647 nm)
Basalt	1.52 + 0.00092i	1.52 + 0.001i
JSC Mars-1	1.5 + 0.01i	1.5 + 0.001i

of two martian dust analogs, namely, basalt and JSC Mars-1 simulant [Dabrowska et al (2015)]. In table 1, we present the refractive index of the samples. The measurements are performed at 448 and 647 nm. As shown, the maximum of the degree of linear polarization for incident unpolarized light for the basalt sample shows higher values at 647 nm than at 488 nm i.e. they present a red polarization color. That seems to be also the color for silicate-type samples with low iron content as shown in many of the samples presented in the Amsterdam-Granada Light Scattering Database ([Muñoz et al. (2012)]).The imaginary part of the refractive index of basalt show a flat wavelength dependence. However, the JSC Mars-1 that presents a significantly higher imaginary part of the refractive index at 488 nm than at 647 nm shows a blue polarization color. The polarization color is directly dependent on the refractive index of the particles showing a red polarization color those particles with a flat dependence of the imaginary part of the refractive index at visible wavelengths and blue polarization color if it is significantly higher at blue than at red wavelengths.

References

[Clancy et al (1995)] Clancy, R.T., Lee, S.W., Gladstone, G.R, McMillan, W.W.,Roush, T., 1995, JGR, 100, 5251-5263.

[Dabrowska et al (2015)] Dabrowska, D.D., Muñoz, O., Moreno, F., Ramos. J.L., Martinez-Frias, J., Wurm., G. 2015. Icarus, 250, 83.

[Mishchencko et al. (2010)] Mishchenko, M.I., Rosenbush, V.K., Kiselev, N.N., et al. (2010), Polarimetric remote sensing of solar system objects. Akademperiodyka, Kyiv.

[Muñoz et al. (2010)] Muñoz, O. Moreno, F., Guirado, D., Ramos, J. L., López, A., Girela, F., Jerónimo, J. M., Costillo, L. P., and Bustamante, I. 2010. JQSRT, 111, 187-196.

[Muñoz et al. (2011)] Muñoz, O.; Moreno, F.; Guirado, D.; Ramos, J.L.; Volten, H.; Hovenier, J.W. The IAA Cosmic Dust Laboratory: experimental scattering matrices of clay particles. Icarus, vol. 211, pp. 894-900, 2011.

[Muñoz et al. (2012)] Muñoz, O.; Moreno, F.; Guirado, D.; Dabrowska, D.D.; Volten, H.; Hovenier, J.W. The Amsterdam-Granada Light Scattering Database. JQSRT, vol. 113(7), pp. 565-574, 2012.

[Pollack et al (1973)] Pollack, J.B., Toon, O.B., Khar, B.N. 1973. Icarus 19, 372-389.

EPSC Abstracts
Vol. 11, EPSC2017-338, 2017
European Planetary Science Congress 2017

Spectro-polarimetry of fine-grained ice and dust samples measured in the laboratory

O. Poch (1), R. Cerubini (1), H. M. Schmid (2), A. Pommerol (1), N. Thomas (1), N. Carrasco (3, 4), C. Szopa (3)

(1) NCCR PlanetS and Physikalisches Institut, University of Bern, Switzerland (olivier.poch@gmail.com),
(2) NCCR PlanetS, Institute for Astronomy, ETH Zurich, Switzerland
(3) Université Versailles St-Quentin; Sorbonne Universités, UPMC Univ. Paris 06; LATMOS, CNRS, France
(4) Institut Universitaire de France

1. Introduction

Many objects of the Solar System have been observed in polarized light [1]. The polarization of the light is very sensitive to the size, morphology, porosity and composition of the scattering particles. As a consequence, polarimetric observations could significantly complement observations performed in total light intensity, providing additional constraints to interpret remote sensing observations.

2. Methods

Here, we present measurements performed in the laboratory of the University of Bern on carefully characterized ice/dust samples to provide reference spectro-polarimetric data. We use a Stokes polarimeter to measure the Stokes parameters describing the polarization of the visible light scattered by ice/dust samples illuminated with a randomly polarized light simulating the star light. The polarization is retrieved at multiple phase angles (1.5-30°) and wavelengths (400-900 nm), allowing to study the shape of the polarimetric phase curves and their spectral dependence. We are performing these measurements on surfaces made of water ice particles having different grain sizes and porosities, as well as mineral/organic dusts, pure or mixed together, as analogues of planetary or small bodies surfaces.

3. Results

For example, Figure 1 shows the degree of polarisation in the light scattered by a flat layer of *tholins* particles, analogues of extraterrestrial complex organic matter, produced from a gas mixture of N_2:CH_4 (95:5) at LATMOS [2]. These tholins are brown-coloured spherical particles of about 300 ± 200 nm. We found that their polarization phase curve strongly depends on the wavelength: the negative branch of polarization is much broader at 530 nm −a wavelength close to the size of the particles, than at 625 and 810 nm. This observation indicates that spectro-polarimetry can be a tool to infer the size of coloured particles.

These results provide interesting inputs to complement theoretical models and predict or interpret spectro-polarimetric properties of Solar System objects and eventually circumstellar disks.

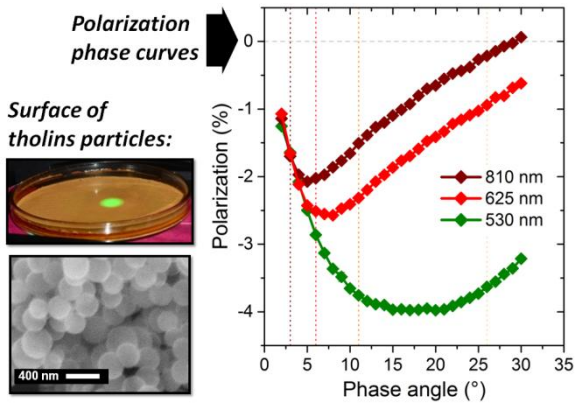

Figure 1: Example of spectro-polarimetric measurements on a surface of *tholins* particles.

Acknowledgements

The authors thank the National Center for Competence in Research ‘‘PlanetS’’ of the Swiss National Science Foundation for funding this project.

References

[1] Kolokolova, L., Hough, J., Levasseur-Regourd, A-C., (2015), Polarimetry of stars and planetary systems, Cambridge University Press, 2015

[2] Carrasco, N., *et al.*, (2009), Chemical characterization of tholins: Solubility, Morphology and Molecular Structure revisited., *J. of Phys. Chem. A* 113, 11195-11203.

EPSC Abstracts
Vol. 11, EPSC2017-412, 2017
European Planetary Science Congress 2017

Asteroid polarimetry as a tool to distinguish rare taxonomic types

I.N. Belskaya (1), S. Fornasier (2), G.P. Tozzi (3), R. Gil-Hutton (4), A. Cellino (5), K. Antonyuk (6), Yu. N. Krugly (1), A.N. Dovgopol(1), S. Faggi (3)

(1) Institute of Astronomy, V.N. Karazin Kharkiv National University, Ukraine (Irina@astron.kharkov.ua), (2) LESIA, Observatoire de Paris, PSL Research University, CNRS, Univ. Paris Diderot, Sorbonne Paris Cité, UPMC Univ., France, (3) INAF – Oss. Astrofisico di Arcetri, Firenze, Italy, (4) CASLEO and San Juan National University, Argentina, (5) INAF – Oss. Astrofisico di Torino, Italy, (6) Crimean Astrophysical Observatory, Nauchny, Crimea

Abstract

The majority of asteroids observed so far show polarimetric phase angle behaviours close to the average phase curve of the corresponding class. Using polarimetric data it is possible to distinguish several types of asteroids which are difficult to distinguish based on spectral data alone.

1. Introduction

Polarimetric measurements can be an effective tool for asteroid taxonomy. It was shown that with respect to spectral reflectance data, polarimetry provides a complementary approach to asteroid classification [1,2]. Extensive observational campaigns in the last decade considerably increased the number of asteroids with known polarimetric measurements (e.g. [3-5]). We have analysed the available data to compare the polarimetric parameters of the main composition classes.

2. Results

We looked through all data [5,6] and selected the measurements in the V and R filters, and also in the G-filter which is close to the V filter. We consider only those measurements of linear polarization having an accuracy ≤0.2% (with a few exceptions for $P_r \geq 2\%$ for which $\sigma \leq 0.3\%$ was accepted). The final data-set includes measurements for 337 asteroids. We have plotted the combined polarization phase curves for main compositional types of asteroids. For the purpose we consider only those asteroids for which classifications are unambiguous and compatible in various taxonomic schemes. We found that the majority of asteroids measured so far show polarimetric behaviour very close to the average polarization phase curve found for the corresponding taxonomic class. There are less than 10% asteroids whose polarimetric properties noticeably deviate from the average polarization phase curve. The obtained average polarization-phase dependences for a particular compositional type are shown in Fig.1 and Fig.2. Different polarimetric behaviors for different asteroid classes are well-seen. Moreover, asteroids of similar albedos (e.g. P and F, K and L, A and V types) may have different polarization curves.

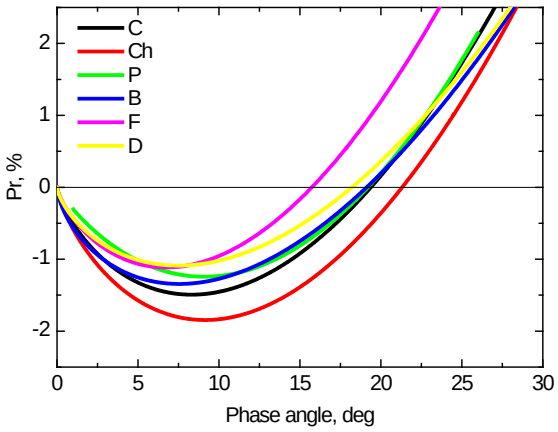

Figure 1: Average polarization-phase curves for low albedo taxonomic types.

Low-albedo types. Polarimetric properties of the F-type asteroids are completely different from other classes due to their unusually small inversion angles (Fig.1). The Ch and Cgh classes are characterized by the deepest negative polarization branches. Asteroids of the C and P classes have similar inversion angles but different depth of negative polarization which can be used to distinguish between them. The D-type asteroids show the smallest depth of negative

polarization like F-asteroids, but larger inversion angles.

Moderate-albedo types. Asteroids of the S-complex have rather homogeneous polarimetric properties. The M-type asteroids have deeper and wider negative polarization branch compared to the S- and K-type asteroids. Asteroids of K- and L-types show different polarization curves and can be distinguished on the basis of polarimetric behaviour alone (Fig.2). Deep negative branch with extremely large inversion angle is a distinct feature of the majority of measured L-type asteroids.

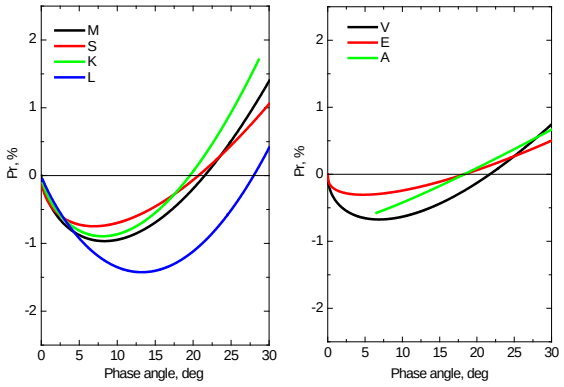

Figure 2: Average polarization-phase curves for moderate (left) and high-albedo (right) taxonomic types.

High-albedo types. The measured E-type asteroids show very similar polarization phase-angle behaviors while the diversity within the A class is evident. The average phase curve for the A-class is not well-defined due to lack of observations at small phase angles. The V-type asteroid (4) Vesta has a wider negative polarization branch compared to E and A-classes.

3. Conclusions

We have shown that using polarimetric data it is possible to refine asteroid taxonomy. The polarimetric data allow to distinguish low, moderate and high-albedo types within the X-complex, and Ch, F, L, K asteroids characterizing by particular polarimetric properties. The observed similarity of the polarization phase curves for asteroids belonging to the same taxonomic class suggest that polarimetric behaviour is intimately related to surface composition.

References

[1] Goidet-Devel, B., Renard, J. B., and Levasseur-Regourd, A.-C. Polarization of asteroids. Synthetic curves and characteristic parameters. Planet. Space Sci, Vol. 43, 779-786. 1995.

[2] Penttilä, A., Lumme, K., Hadamcik, E., and Levasseur-Regourd, A.-C. Statistical analysis of asteroidal and cometary polarization phase curves. Astron. Astrophys., 432, 1081-1090, 2005.

[3] Cellino, A., Bagnulo, S., Tanga, P., Novakovic, B., and Delbò, M. A successful search for hidden Barbarians in the Watsonia asteroid family. MNRAS, 439, L75-L79, 2014.

[4] Fornasier, S., Beskaya, I.N., Shkuratov, Yu.G., Pernechele, C., Barbieri, C., Giro, E., and Navasardyan, H. 2006. Polarimetric survey of asteroids with the Asiago telescope. Astron. Astrophys., 455, 371-377, 2006.

[5] Gil-Hutton, R., Cellino, A., Bendjoya, Ph. Polarimetric survey of main-belt asteroids. IV. New results from the first epoch of the CASLEO survey. Astron. Astrophys., 569, id.A122, 6 pp., 2014.

[6] Lupishko D. F. 2014. Asteroid Polarimetric Database V8.0. NASA Planetary Data System, EAR-A-3-RDR-APD-POLARIMETRY-V8.0.

EPSC Abstracts
Vol. 11, EPSC2017-416, 2017
European Planetary Science Congress 2017

Laboratory studies of light scattering by well-controlled and characterized ice samples

N. Thomas(1), A. Pommerol(1), O. Poch(1), B. Jost(1), and Z. Yoldi(1)
(1)Physikalisches Inst., University of Bern, Sidlerstrasse 5, CH-3012 Bern, Switzerland (nicolas.thomas@space.unibe.ch).

Abstract

Over the past 8 years, we have developed LOSSy – the Laboratory for Outflow Studies of Sublimating Materials - at the University of Bern. The aim of this lab. is to produce ice and dirty ice samples that are reproducible and that can be characterized with an array of different instruments. This has primarily been for planetary science although application to Earth-orbiting remote sensing and studies of proto-planetary discs have also been looked at.

Ice particles of varying sizes can be produced using different setups. These setups use nebulizers with different characteristics. The surface structure of the resulting material can be investigated using scanning electron microscopy and optical coherence tomography. A spectro-goniometer (PHIRE-2) can then be used to determine the reflectance properties over the full hemisphere. Both the sample and the goniometer can be maintained at low temperature (typically -30C) during these measurements. A thermal vacuum chamber (SCITEAS) is also available for space simulation and VIS-NIR hyperspectral measurements can be made while the sample evolves under different conditions. A system has also been developed to measure the polarization of icy samples at multiple wavelengths in the visible and from 3 to 30° phase angle (with direct application to icy satellite observations). Approaches to determine the properties of the samples at sub-mm wavelengths have also been developed. The presentation will show some of our latest results.

Examples

We have studied a large number of icy samples prepared using our standardised sample preparation systems called SPIPA [1]. The PHIRE-2 spectro-goniometer measurements [2] are now produced in a standardized format (PDS compatible) and many are now free to use through the DACE platform [3] of the National Center for Competence in Research programme, PlanetS. Data at low phase angle can now be acquired easily with high signal to noise [4].

Figure 1 shows the DACE interface with our goniometer measurements. Hapke parameter fits to the data can almost be made.

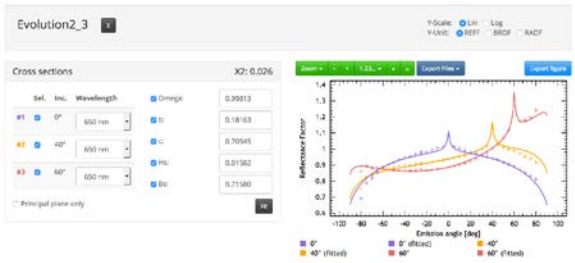

Figure 1 The DACE interface to our database of bidirectional reflectance distribution function.

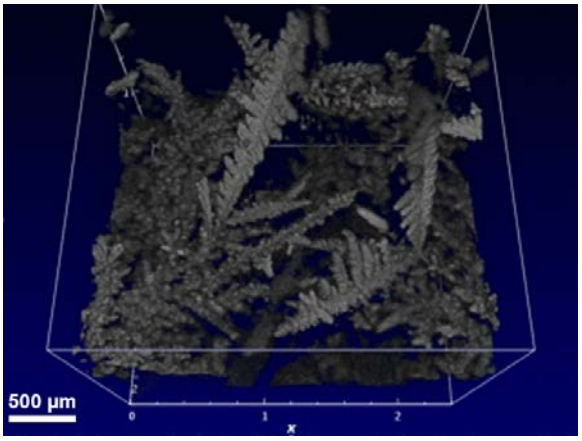

Figure 2 The high precision characterization of surfaces can be performed with the Optical Coherence Tomography equipment. Here an example of water frost is shown.

While preparation is important characterization is also of great significance. In Figure 2 an example from our Optical Coherence Tomography experiment (OCTOPUS) is shown. This provide 6 µm resolution

contactless imagery of surfaces and allows us to characterize surface structure at scales only slightly larger than the wavelength of the light used for goniometric investigations. Our equipment is transportable allowing us to bring samples to a cryo-SEM for further higher resolution characterization [4].

The POLICES equipment is a novel development with the Bern laboratory and is being used to study polarization of many materials including materials of direct relevance for the investigation of comets. An example is shown in Figure 3. Whilst there remains some work to be done to improve aspects of the set-up, this equipment is functional and already producing accurate results.

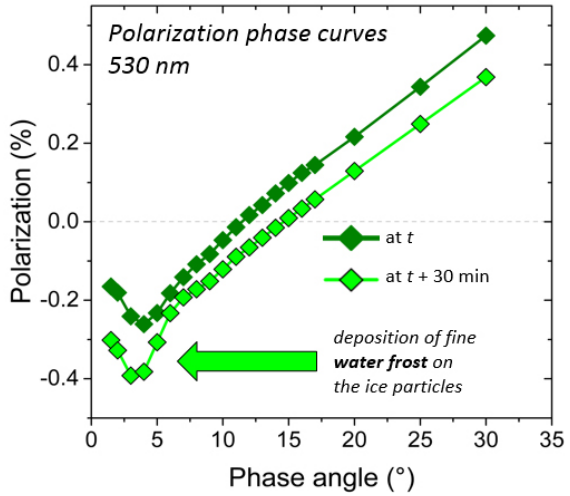

Figure 3 Polarization phase curve of water ice particles using the SPIPA preparation system.

The data can be used for studies of carbon-rich dust/ice mixtures with applications to comets [5]. We are also performing near-infrared hyperspectral monitoring of evolving surfaces within the SCITEAS system [6]. The laboratory is a powerful tool for supporting interpretation of planetary remote-sensing observations. The techniques used are also being used to prepare samples for other experiments [e.g. 7]. We are open to collaboration on a variety of topics.

Acknowledgements

The team from the University of Bern is supported through the Swiss National Science Foundation and through the NCCR PlanetS.

References

[1] Poch, O. et al., Icarus, 267, 154-173, 2016
[2] Jost, B. et al., Icarus, 225, 352-366, 2013
[3] https://dace.unige.ch
[4] Jost, B. et al., Icarus, 264, 109-131, 2016
[5] Jost, B. et al., PSS, submitted, 2017
[6] Yoldi, Z. et al. this conference
[7] Galli, A. et al., PSS, 126, 63-71, 2016.

EPSC Abstracts
Vol. 11, EPSC2017-424-1, 2017
European Planetary Science Congress 2017

Multiple light scattering in planetary regoliths: Numerical methods and their validation

K. Muinonen (1,2), J. Markkanen (1), T. Väisänen (1), and A. Penttilä (1)
(1) Department of Physics, University of Helsinki, Finland, (2) Finnish Geospatial Research Institute FGI, Masala, Finland
(karri.muinonen@helsinki.fi / Fax: +358-2941-50610)

Abstract

We devise numerical methods for the computation of light-scattering characteristics for planetary regoliths of airless Solar System objects. Using microscopic systems of small particles, we validate the numerical methods through a detailed comparison to the results obtained using exact electromagnetic methods. We conclude that the novel numerical methods allow for a quantitative interpretation of the spectroscopy, polarimetry, and photometry of asteroids and other airless Solar System objects.

1. Introduction

In asteroid photometry and polarimetry, two striking phenomena are observed at small solar phase angles (the Sun-Object-Observer angle). First, a nonlinear increase of brightness is observed towards zero phase in the magnitude scale (the opposition effect). Second, the scattered light is observed to be partially linearly polarized parallel to the Sun-Object-Observer plane (the negative polarization surge). Asteroid UV-Vis-NIR spectra show varying trends and absorption bands due to, for example, olivine and pyroxene minerals, as well as carbon and iron compounds. Generally, these spectra are functions of the phase angle.

Electromagnetic scattering (or light scattering) in a macroscopic particulate medium composed of microscopic particles is an unsolved computational problem. This results in the absence of quantitative direct and related inverse methods to interpret fundamental astronomical observations of asteroids. We report advances in the theoretical understanding of light scattering by macroscopic particulate media. We aim at distributing open software for the computation of UV-Vis-NIR spectra as well as photometric and polarimetric characteristics for asteroids, cometary nuclei, and other small Solar System objects.

2. Numerical methods

We have generalized the numerical method of radiative transfer and coherent backscattering (RT-CB, [1,2]) for densely packed discrete random media of scattering and absorbing particles [3]. Starting from the approach followed by Zurk et al. [4], we incorporate, into RT-CB, incoherent extinction, scattering, and absorption properties of a volume element. That allows us to remove the shortcomings due to the assumption of independent scattering in a sparse random medium. In its most general order-of-scattering form entitled R^2T^2 ("RT squared", radiative transfer with reciprocal transactions, [3]), interactions among the volume elements are computed exactly using FaSTMM, the fast superposition T-matrix method [5]. We have developed efficient software for both RT-CB entailing incoherent interactions as well as R^2T^2. Finally, we have generalized the open-source SIRIS geometric-optics software for specular and diffuse interactions [6] to incorporate incoherent volume-element scattering characteristics.

3. Results and discussion

Our framework allows for a quantitative end-to-end analysis spanning from modeling the single-particle scattering measurements to modeling multiple scattering in macroscopic media of particles (Penttilä et al., this meeting).

We point out that the modeling framework is already utilized for analyzing space-weathering effects (Markkanen et al., this meeting) and meteorite spectrometry (Martikainen et al., this meeting), as well as in modeling multiple scattering by high-albedo planetary-regolith analog samples of silica spheres measured in the laboratory (Väisänen et al., this meeting). In the present work, we offer a detailed comparison of computations using the R^2T^2 and RT-CB methods and the exact FaSTMM method. We show one example comparison in Figs. 1 and 2 for a close-packed spherical medium of small ice particles.

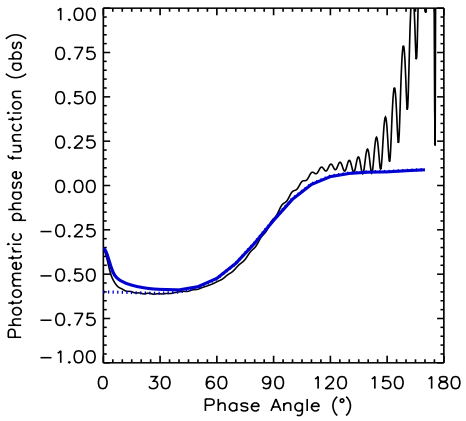

Figure 1: Scattering by a spherical particulate medium of radius 4 μm with 25% volume fraction of 0.2-μm spherical particles with refractive index 1.31. The wavelength is 0.6283 μm. The black solid curves depict the exact Superposition T-matrix results [5], and the blue solid curves depict our new R^2T^2 results (radiative transfer with reciprocal transactions; [3]). The intensity comparison is in absolute units.

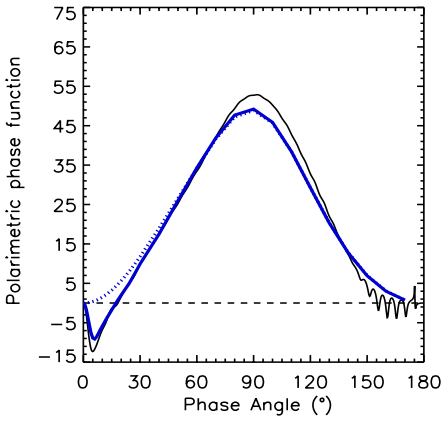

Figure 2: As in Fig. 1 for the degree of linear polarization for incident unpolarized light (in %).

4. Conclusion

We have developed advanced numerical methods for electromagnetic scattering in planetary regoliths and make them openly available. In the near future, we expect major advances in synoptic modeling of asteroid UV-Vis-NIR spectra, photometry, and polarimetry.

5. Acknowledgements

Research supported, in part, by the ERC Advanced Grant 320773.

References

[1] Muinonen, K.: Coherent backscattering of light by complex random media of spherical scatterers: Numerical solution. Waves in Random Media, 14, pp. 365-388, 2004.

[2] Muinonen, K., Mishchenko, M. I., Dlugach, J. M., Zubko, E., Penttilä, A., and Videen, G.: Coherent backscattering numerically verified for a finite volume of spherical particles. Astrophys. J., 760, 118, pp. 1-11, 2012.

[3] Muinonen, K., Markkanen, J., Penttilä, A., Väisänen, T., and Peltoniemi, J.: Multiple scattering by dense random media: Numerical solution, URSI Electromagnetic Theory Symposium EMTS'16, 14-18 August 2016, pp. 400-403, 2016.

[4] Zurk, L. M., Tsang, L., Ding, K. H., and Winebrenner, D. P.: Monte Carlo simulations of the extinction rate of densely packed spheres with clustered and nonclustered geometries. J. Opt. Soc. Am. A, 12, pp. 1772-1781, 1995.

[5] Markkanen J. and Yuffa A. J.: Fast superposition T-matrix solution for clusters with arbitrarily-shaped constituent particles. JQSRT, 189, pp. 181-188, 2017.

[6] Muinonen, K., Nousiainen, T., Lindqvist, H., Munoz, O., and Videen, G.: Light scattering by Gaussian particles with internal inclusions and roughened surfaces using ray optics. JQSRT, 110, pp. 1628-1639, 2009.

EPSC Abstracts
Vol. 11, EPSC2017-477-1, 2017
European Planetary Science Congress 2017

Asteroid lightcurve inversion with Bayesian inference: Reference phase curves

K. Muinonen (1,2), J. Torppa (3), X. Wang (4), A. Cellino (5), J. Martikainen (1), O. Wilkman (2), M. Gritsevich (1), and A. Penttilä (1)
(1) Department of Physics, University of Helsinki, Finland, (2) Finnish Geospatial Research Institute FGI, Masala, Finland (karri.muinonen@helsinki.fi / Fax: +358-2941-50610), (3) Space Systems Finland, Espoo, Finland, (4) Yunnan Observatories, Kunming, China, (5) INAF, Osservatorio Astrofisico di Torino, Pino Torinese, Italia.

Abstract

An asteroid's lightcurve, i.e., its observed disk-integrated brightness as a function of time, depends on the shape and spin state of the asteroid, as well as its surface scattering properties. It follows that these properties can be estimated from the observations, to an extent allowed by a given data set. The phase curve of the asteroid refers to the dependence of disk-integrated brightness on the phase angle (the Sun-Object-Observer angle). In the present work, we study reference phase curves that are extrapolated to equatorial illumination and observation of the given asteroid. We show that the reference phase curves, with realistic error bars, can be efficiently derived through statistical lightcurve inversion. These phase curves can have substantial value in asteroid taxonomy.

1. Introduction

Lightcurve inversion proceeds conventionally as follows (e.g., [1]). It is reasonable to derive the rotation period with a simplified shape model and a small number of trial pole orientations. Once the period is available, the pole orientation can be refined with a general convex shape model represented by a spherical harmonics expansion for the Gaussian surface density. Once the Gaussian surface density is available, the actual convex shape is constructed as a solu-tion of the Minkowski problem.

In the present work, we devise statistical inverse methods for the retrieval of rotation periods, pole orientations, convex shapes, and scattering properties from the photometric observations. This entails a complete assessment of the uncertainties in the abovementioned physical parameters. We consider conventional photometric data composed of dense lightcurves [1] as well as sparse data mimicking the ongoing observations of the ESA Gaia mission [2]. Our inverse methods comprise both MCMC (Markov chain Monte Carlo) and importance samplers, building upon the recent advances with the Lommel-Seeliger ellipsoids [3,4], the Monte Carlo virtual-photometry method [5], and an efficient numerical surface scattering model [6].

2. Numerical methods

In what follows, we adopt either a triaxial ellipsoid shape model or a general convex shape model, describing the shape by the spherical harmonics expansion for the Gaussian surface density. In the statistical inverse problem, it is our goal to characterize the Bayesian a posteriori probability density for the unknowns. For the ellipsoid model, this involves a small number of unknowns, whereas, for the convex model, this involves high-dimensional forward models with several dozens to hundreds of unknowns. All of the inverse methods are based on the concept of virtual observations, that is, simulated observations obtained by adding random noise to the true observations, and, subsequently, on the virtual least-squares solutions available from the best fits to the virtual observations.

First, in the case of extensive observations, we provide an independence-like importance sampler based on kernel estimation and debiasing of the probability density for the virtual least-squares parameters. Second, in the case of scarce observations, we provide a random-walk MCMC sampler based on the convolution of the probability density for the virtual least-squares parameters by itself, as well as, a random-walk importance sampler based on the same con-volved probability density.

3. Results and discussion

In Figs. 1 and 2, we highlight the interrelation between conventional asteroid phase curves and reference phase curves in the case of sparse photometry simulated for the Gaia mission. For the

phase curves (Fig. 1), the large variation of the phase curve points is due to the considerably different viewing geometry for the individual phase curve points. The caveat is removed in Fig. 2 by the introduction of the reference viewing geometry: the reference phase curves are smooth from one epoch to another. Finally, we can see that the reference phase curves pertaining to the lightcurve maxima have smaller slopes than the reference phase curves pertaining to the mean brightnesses. In Figs. 1 and 2, the error bars are small and fall inside the plotting symbols.

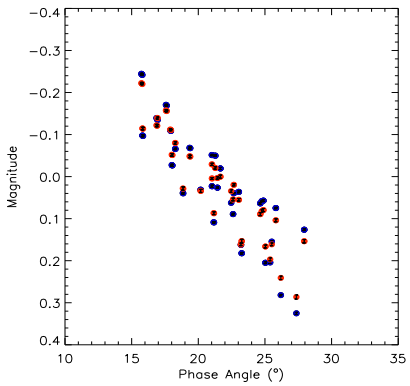

Figure 1: Phase curves corresponding to the mean (blue) and maximum brightness (red) as computed using the sample models at the epoch of each photometric point.

4. Conclusion

We conclude that the present inverse methods promise to settle the issue of missing statistical methods for uncertainty estimation in the lightcurve inversion problem. They allow for efficient retrieval of reference phase curves that can be utilized in asteroid taxonomy. In the future, computational tools based on the present inverse methods will be available through a web-based Gaia Added Value Interface.

5. Acknowledgements

Research supported, in part, by the ERC Advanced Grant 320773.

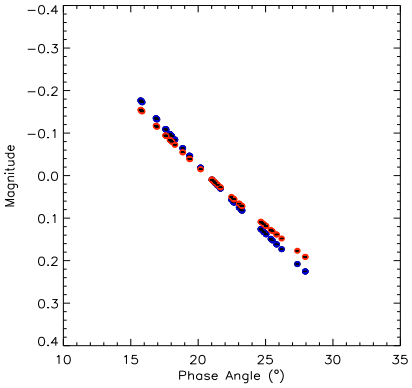

Figure 2: As in Fig. 1 for the reference phase curves.

References

[1] Torppa, J., Hentunen, V-P., Pääkkönen, P., Kehusmaa, P., and Muinonen, K.: Asteroid shape and spin statistics from convex models. Icarus, 198, pp. 91-107, 2008.

[2] Santana-Ros, T., Bartczak, P., Michałowski, T., Tanga, P., and Cellino, A.: Testing the inversion of the asteroids' Gaia photometry combined with ground-based observations. Mon. Not. Roy. Astron. Soc., 450, pp. 333-341, 2015.

[3] Cellino, A., Muinonen, K., Hestroffer, D., and Carbognani, A.: Inversion of sparse photometric data of asteroids using triaxial ellipsoid shape models and a Lommel-Seeliger scattering law. Planet. Space Sci., 118, pp. 221-226, 2015.

[4] Muinonen, K., Wilkman, O., Cellino, A., Wang, X., and Wang, Y.: Asteroid lightcurve inversion with Lommel-Seeliger ellipsoids. Planet. Space Sci., 118, pp. 227-241, 2015.

[5] Wang, X., Muinonen, K., Wang, Y., Behrend, R., Goncalves, R., Oey, J., Antonini, P., Demeautis, C., Manzini, F., Damerdji, J., Montier, J., Klotz, A., Leroy, A., and Ganand, G.: Photometric analysis for the spin and shape parameters of the C-type main-belt asteroids (171) Ophelia and (360) Carlova. Astron. Astrophysics, 581, A55, 2015.

[6] Wilkman, O., Muinonen, K., and Peltoniemi, J.: Photometry of dark atmosphereless planetary bodies: an efficient numerical model. Planet. Space Sci., 118, pp. 250-255, 2015.

EPSC Abstracts
Vol. 11, EPSC2017-544-1, 2017
European Planetary Science Congress 2017

Multiple scattering modeling pipeline for spectroscopy, polarimetry, and photometry of airless Solar System objects

A. Penttilä (1), T. Väisänen (1), J. Markkanen (1), J. Martikainen (1), M. Gritsevich (1), and K. Muinonen (1,2)
(1) Department of Physics, University of Helsinki, Finland, (2) Finnish Geospatial Research Institute FGI
(antti.i.penttila@helsinki.fi)

Abstract

We are developing a set of numerical tools that can be used in analyzing the reflectance spectra of granular materials such as the regolith surface of atmosphereless Solar System objects. Our goal is to be able to explain, with realistic numerical scattering models, the spectral features arising when materials are intimately mixed together. We include the space-weathering-type effects in our simulations, i.e., mixing of the host mineral locally with small inclusions of another material in small proportions.

1. Introduction

We are combining a set of numerical tools to analyze the reflectance spectra of granular materials. Our motivation for this study comes from the present lack of such tools when it comes to intimate mixing of materials, including space-weathering effects with nano- or micron-sized inclusions in the host matrix. The current common practice is to apply a semi-physical approximate model such as some variation of the Hapke models (e.g., [1]) or the Shkuratov model [2]. These models are expressed in a closed form so that they are relatively fast to apply. They are based on simplifications on the radiative transfer theory. The problem is that the validity of the model is not always guaranteed, and the derived physical properties related to particle scattering properties can be unrealistic [3]. The Hapke space-weathering model does not include correct size dependence for the nanophase iron inclusions [4].

2. The analysis pipeline

Our numerical tool consists of individual scattering simulation codes and a main program that chains them together, calling the codes and converting the output of one code as input for the next code. The chain for analyzing a macroscopic target with space-weathered mineral would go as follows:

1. Scattering properties of small inclusions inside an absorbing host matrix can be derived using exact methods solving the Maxwell equations of the system. From the scattering properties, we use the so-called incoherent fields and the corresponding incoherent Mueller matrices as input for the next step [5, 6].

2. Scattering by a single regolith grain is solved using a geometrical optics method accounting for surface reflections, internal absorption, and possibly the internal diffuse scattering (See Fig. 1 for SIRIS geometrical optics method).

3. The radiative transfer simulation is executed inputting the regolith grains in the previous step as the basic scatterers in a macroscopic spherical, planar, or arbitrary shaped volume element (See Fig. 2 for a schematic presentation of this chain).

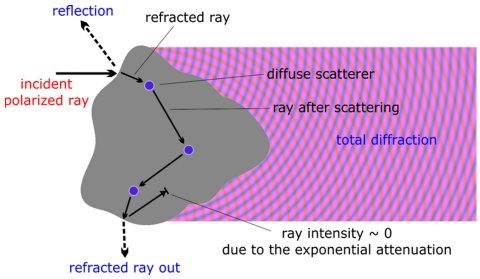

Figure 1: A presentation of the scattering concepts in the SIRIS geometrical optics code by Muinonen et al.[7].

For the most realistic asteroid reflectance model, the abovementioned chain would produce the scattering properties of a planar surface element. Then, a shadowing simulation over the target surface elements would be considered, and finally the asteroid phase

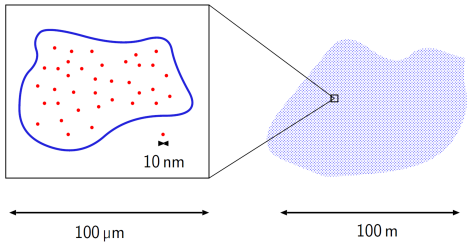

Figure 2: A schematic presentation of the chain of scattering computations for an macroscopic object (in the right) constituting of regolith grains that can include nanoscale internal diffuse scatterers (in the left).

function would be solved by integrating the bidirectional reflectance distribution function of the planar element over the object's realistic shape model.

For mixing intimately two or more minerals with sizes larger than the wavelength of light, the first step of the abovementioned chain would be omitted. Instead, the single grain properties would be computed for every material, and then averaged into imaginary average grain. The macroscopic properties would be computed following the recipe above.

The tools in the proposed chain already exist, and practical task for us is to tie these together into an easy-to-use public toolchain. We plan to open the abovementioned toolchain as a web-based open service. In detail, we are building this chain in a dedicated (virtual) server, using Django application server and Python environment for the chain main functionality. The individual programs to be ran under the chain can still be programmed with Fortran, C, or other.

Acknowledgements

The authors acknowledge the financial support from the European Research Council, Advanced Grant No. 320773 entitled Scattering and Absorption of Electromagnetic Waves in Particulate Media (SAEMPL). The computational resources are provided by CSC — IT Center for Science Ltd., Finland.

References

[1] B. Hapke. Bidirectional reflectance spectroscopy: 6. Effects of porosity. *Icarus*, 195(2):918–926, 2008.

[2] Yu. Shkuratov, L. Starukhina, H. Hoffmann, and G. Arnold. A model of spectral albedo of particulate surfaces: Implications for optical properties of the Moon. *Icarus*, 137(2):235–246, 1999.

[3] Y. Shkuratov, V. Kaydash, V. Korokhin, Y. Velikodsky, D. Petrov, E. Zubko, D. Stankevich, and G. Videen. A critical assessment of the Hapke photometric model. *J Quant Spectrosc Radiat Transf*, 113(18):2431–2456, 2012.

[4] P.G. Lucey and M.A. Riner. The optical effects of small iron particles that darken but do not redden: Evidence of intense space weathering on mercury. *Icarus*, 212(2):451–462, 2011.

[5] K. Muinonen, J. Markkanen, A. Penttilä, A. Virkki, and D. Mackowski. Multiple scattering by dense random media: Volume-element extinction. In *URSI Electromagnetic Theory Symposium EMTS'16*, pages 751–754, Espoo, Finland, 2016.

[6] K. Muinonen, J. Markkanen, A. Penttilä, T. Väisänen, and J. Peltoniemi. Multiple scattering by dense random media: Numerical solution. In *URSI Electromagnetic Theory Symposium EMTS'16*, pages 400–403, Espoo, Finland, 2016.

[7] K. Muinonen, T. Nousiainen, H. Lindqvist, O. Muñoz, and G. Videen. Light scattering by Gaussian particles with internal inclusions and roughened surfaces using ray optics. *J Quant Spectrosc Radiat Transf*, 110:1628–1639, 2009.

EPSC Abstracts
Vol. 11, EPSC2017-554-1, 2017
European Planetary Science Congress 2017

Experimental light scattering with a novel Mueller matrix scatterometer

A. Penttilä (1), G. Maconi (1), **I. Kassamakov** (1), M. Gritsevich (1), P. Helander (1), T. Puranen (1), A. Salmi (1), E. Hæggström (1), and K. Muinonen (1,2)
(1) Department of Physics, University of Helsinki, Finland, (2) Finnish Geospatial Research Institute FGI
(antti.i.penttila@helsinki.fi)

Abstract

We describe a setup for measuring the full angular Mueller matrix profile of a single mm- to µm-sized sample, and verify the experimental results against a theoretical model. The scatterometer has a fixed or levitating sample, illuminated with a laser beam whose full polarization state is controlled. The scattered light is detected with a combination of wave retarder, linear polarizer, and photomultiplier tube that is attached to a rotational stage.

1. Introduction

Measuring scattering properties of different targets is important for material characterization, remote sensing applications, and for verifying theoretical results. Furthermore, there are usually simplifications made when we model targets and compute the scattering properties, e.g., ideal shape or constant optical parameters throughout the target material. Experimental studies can help us in understanding the link between the observed properties and computed results.

Experimentally derived Mueller matrices of particles can be used as input for larger-scale scattering simulations, e.g., radiative transfer computations. This method allows us to bypass the problem of using idealized model for single-particle properties. There are publicly available studies of the scattering properties of particles, e.g., the Granada light scattering database [1]. With our scatterometer, we aim to offer similar material for single, small (down to µm-scale) targets. While other sources usually offer ensemble- and orientation-averaged particle properties, we will be able to measure individual particles with controlled or known orientation.

2. Scatterometer

The measurement can be done in several colors in the visual band. The measurement head comprises a combination of wave retarder, linear polarizer, and photomultiplier tube. One or several of these heads are attached to a rotational stage, so that a range of scattering angles can be covered. The whole system is divided into two chambers that are divided by partition walls. The walls are covered with non-reflecting fabric with only a small pinhole for the incident beam to avoid excess reflections. All the optical components shaping the incident beam are seated in the right chamber (b in Fig. 1), and the scatterer and the detectors are located in the left chamber (a in Fig. 1). Furthermore, there is a second pinhole on the leftmost wall for the forward beam to be guided out from the measurement chamber and into a beam trap.

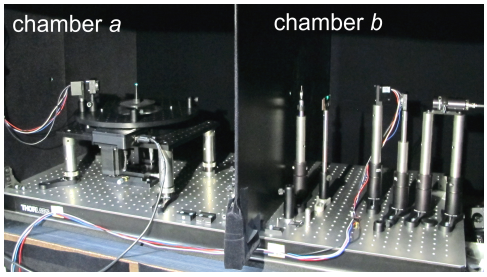

Figure 1: Image of the current development version of the scatterometer. The sample is standing on a static conic pedestal in this image, and not levitated with the ultrasonic device.

The incident beam is generated with a tunable multimode Argon-krypton laser, with 12 selectable wavelengths ranging from 465 to 676 nm. The laser is placed outside the chambers to avoid excess heat and vibration, and the light is brought in with an optical

fiber. In chamber b (Fig. 1), the beam is expanded, diffused, and shaped after the fiber output to create a speckle-free, collimated constant-intensity beam. The polarization state of the beam is controlled by rotation-controlled linear polarizer and wave retarder. The incident beam is monitored by a photomultiplier tube (PMT) detecting the secondary reflection intensity from the system before the measurement chamber.

The incident beam encounters the scattering target in chamber a (Fig. 1). The target will be controlled with an advanced ultrasonic levitator. The levitator comprises several individually-controlled amplifiers and outputs to generate a complex ultrasound field. The shape of the field can be modified to generate a stable trap or even vortex forces in the trap. We aim to be able to control the target orientation in the trap with the ultrasound field, and the target position and orientation can be monitored using a high-speed camera attached to the system. The ultrasound trap is still under development, and the first tests presented here are executed with the target seated on a thin solid cone pedestal, or with a more simple singe-amplifier levitator.

The detectors, Hamamatsu micro-PMTs, are mounted radially towards the target on a rotational stage. The stage is controlled by a rotation motor with an accuracy of 15'. The current 150-mm radius allows measuring all azimuthal angles except for $\pm 4°$ around the backward scattering direction. With several detectors we can do a simultaneous multi-angle measurement, and by rotating the stage we can increase and sample more densely the angle range. The small physical dimensions of the new micro-PMTs allow us to seat many detectors side-by-side without compromising in the distance to the target too much.

3. Results

We have conducted the first calibration measurements with the scatterometer. The first set of measurements are done with one wavelength at 514 nm, with one detector that is rotated over the sample, and with linear polarizers only. The sample, which is a N-BK7 clear glass sphere from Edmund Optics, diameter $d = 5$ mm and refractive index $n = 1.5$, is mounted on a thin black cone (static sample).

We verify the first measurement set by comparing the angular scattering profile against the theoretical results computed using Mie theory. The Mie results are averaged over a small angular window to accommodate the actual acceptance angle of the detector. For the clear sphere, the symmetries require that $M_{11} = M_{22}$ and that $M_{12} = M_{21}$. In Fig. 2 we can see that the symmetries hold quite well. Also, comparing to model (Mie) results show quite nice agreement.

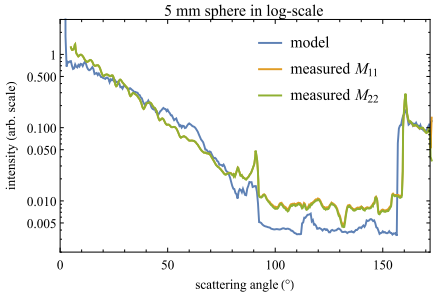

Figure 2: Measurements and model for 5-mm clear static sphere, diagonal elements M_{11} and M_{22}. The measured elements overlap, so the measured M_{11} curve is behind the measured M_{22}.

Acknowledgements

The authors acknowledge the financial support from the European Research Council, Advanced Grant No. 320773 entitled Scattering and Absorption of Electromagnetic Waves in Particulate Media(SAEMPL).

References

[1] O. Muñoz, F. Moreno, D. Guirado, D.D. Dabrowska, H. Volten, and J.W. Hovenier. The Amsterdam–Granada light scattering database. *J Quant Spectrosc Radiat Transf*, 113(7):565–574, 2012.

EPSC Abstracts
Vol. 11, EPSC2017-605, 2017
European Planetary Science Congress 2017

Radiative-transfer modeling for measured scattering properties of a planetary-regolith analog sample

T. Väisänen (1), J. Markkanen (1), E. Hadamcik (2), A.C. Levasseur-Regourd (3), J. Lasue (4), J. Blum (5), A. Penttilä (1) and K. Muinonen (1,6);
(1) Department of Physics, Univ. of Helsinki, Finland, (2) LATMOS/CNRS, Pierre and Marie Curie Univ., France, (3) LATMOS/CNRS, UPMC (Sorbonne Univ.), France, (4) IRAP-CNRS, Univ. of Toulouse, France, (5) IGEP, Brunswick Univ. of Technology, Germany, (6) Finnish Geospatial Research Institute, FGI, Finland, (timo.h.vaisanen@helsinki.fi)

Abstract

Multiple scattering by a planetary-regolith analog surface consisting of closely equisized silica spheres was studied with recently developed Radiative Transfer with Reciprocal Transactions (R^2T^2) and Radiative Transfer Coherent Backscattering with Incoherent interactions (RT-CB-ic). The computed results match the experimental results relatively well, considering that the computer modeling is in early stages.

1 Introduction

In order to do reliable inversion of the properties of the asteroid surface from spectral and polarimetric data, physics-based electromagnetic scattering programs, which work for large and dense media, are needed. The exact methods exist but these methods fail when the media is huge and thus approximate methods need to be developed. For this purpose we have been developing the radiative transfer codes R^2T^2 and RT-CB-ic [1]. To show the current progress of our work, we have modeled a planetary-regolith analog sample using them.

The analog sample is a low-density agglomerate produced by random ballistic deposition (RBP) of almost equisized SiO2 spheres (refractive index n=1.5 and diameter 1.45 $\pm$0.06 µm with Gaussian size distribution). The volume fraction of the sample was 0.15 $\pm$0.03 and the size of the diameter of the cake was about 20 mm and depth 5 mm. The experimental setup and more about the sample can be found in [2] and [3].

The light-scattering properties of the sample were studied using the PROGRA^2-surf experiment which has been developed to provide polarization phase curves which can be compared to remote sensing observations [4].

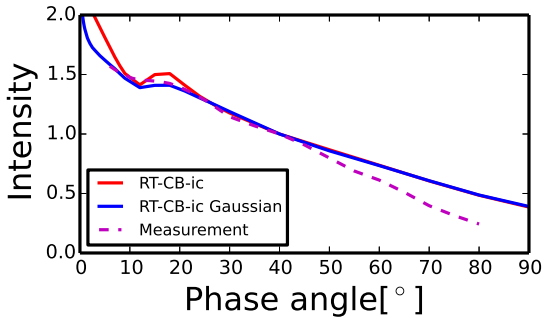

Figure 1: Intensity. Normalized to unity at 40 °

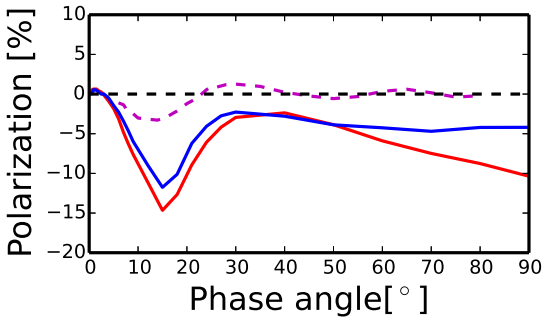

Figure 2: Degree of linear polarization

2 Computational Methods

The computational modeling was done by using radiative transfer codes the RT-CB-ic and the R^2T^2, which use the so the so-called incoherent fields [5], and include the coherent backscattering effect. We have shown that the incoherent field treatment can make the radiative transfer applicable to dense media [1]. The RT-CB-ic is not compute intensive and thus can be run

on a personal computer whereas the R^2T^2 can require a supercomputer if the studied medium and scatterers are large. These methods are work in progress so improvements in the near future are expected.

3 Results

We have computed scattering from a macroscopic spherical medium (volume fraction 0.15) with RT-CB-ic [see Figs. 1 and 2] using single particle size (diameter 1.45 μm, red curve) and Gaussian distribution for the size (mean 1.45 μm with σ=0.02 μm, blue curve), with the refractive index (n = 1.48+0.0001i) which is due to remarks made in [3].

4. Summary and Conclusions

The RT-CB-ic produces relatively well the measurement results although the system is modeled using simple assumptions. The results can get better by tweaking the size distribution of the scatterers and modeling the shape of the media better. Large sphere as a shape of the media was assumed in the computations. The low polarization peak near 15° is a challenge for our methods. The reason for this can be the clustering of the spheres in the sample which is not present in current computational models.

Acknowledgements

We acknowledge the ERC Advanced Grant no. 320773 entitled Scattering and Absorption of Electromagnetic Waves in Particulate Media (SAEMPL). Computational resources were provided by CSC — IT Centre for Science Ltd, Finland.

References

[1] K. Muinonen, J. Markkanen, A. Penttilä, T. Väisänen, J. Peltoniemi, [Abstract], 2016 URSI International Symposium on Electromagnetic Theory (EMTS).

[2] J. Blüm, R. Schräpler, *Physical Review Letters*, 93, 11, 2004

[3] E. Hadamcik, J.-B Renard, J. Lasue, A.C. Levasseur-Regourd, J. Blüm, R. Schäpler, JQSRT, 106, 74-89, 2007

[4] A.C. Levasseur-Regourd et al. *Polarimetry of stars and planetary systems*, CUP, 61-80, 2015

[5] L. M. Zurk, L. Tsang, D. P. Winebrenner, *Radio Science*, 31(4), 1996.

EPSC Abstracts
Vol. 11, EPSC2017-633-1, 2017
European Planetary Science Congress 2017

Numerical analysis of space weathering effects on light scattering by asteroid surfaces

J. Markkanen (1), J. Martikainen (1), A. Penttilä (1) and K. Muinonen (1,2)
(1) Department of Physics, University of Helsinki, Finland (2) Finnish Geospatial Research Institute FGI, National Land Survey, Finland
(johannes.markkanen@helsinki.fi)

Abstract

We analyze the effects of space weathering on light-scattering features of small atmosphereless planetary bodies. We have developed a novel radiative transfer (RT) approach to model light scattering by dense discrete random media. In this work, we combine the RT approach to the geometric optics which allows us to model space-weathering effects on light scattering by planetary surfaces more rigorously that has been possible before.

1. Introduction

Airless planetary bodies are exposed to the space weathering processes such as the energetic solar and cosmic radiation, implantation and sputtering from solar wind particles, and micrometeorite bombardment. Space weathering is known to alter physical and chemical composition of the surface of an airless body. For example, a significant effect of the space weathering is the production of nanophase iron ($npFe^0$) near the exposed surface [1, 2]. This, in turn, impacts the remote light-scattering observables, e.g., the visible and infrared spectra. Typically, space-weathered materials are darker at visible wavelengths but differences in brightness vanish at near infrared. Moreover, the diagnostic absorption bands in the spectrum are much weaker for space-weathered materials.

2. Numerical method

We model light scattering by asteroids with the hierarchical geometric optics (GO) / radiative transfer (RT) approach. The asteroid is assumed to consist of densely packed Gaussian random sphere (GRS) grains of mean size 40 microns. Spherical $npFe^0$ particles are embedded in each grain with the specified packing density. Contributions of the $npFe^0$ particles are treated by the Monte Carlo RT algorithm. Reflections and refractions on the grain surface and propagation in the grain are addressed by the GO. The approach provides the ensemble average phase function which is used in the higher level RT algorithm as an input parameter to compute the scattering characteristics of the entire asteroid.

The mean free path and the volume-element scattering matrix are the input parameters for the higher level RT algorithm. Since the $npFe^0$ inclusions are expected to have a strong contribution to the total scattering, their contribution must be carefully addressed. We compute interactions of the $npFe^0$ particles in the volume element exactly by the fast superposition T-matrix method (FaSTMM) [3] in order to retrieve the incoherent mean free path and the ensemble averaged incoherent scattering matrix [4, 5].

3. Numerical example

Fig. 1 shows an example of calculated spectra with varying $npFe^0$ density for two different size distributions. The asteroid is assumed to be of a GRS shape with a radius of 100 m, and it is composed of 40 microns GRS olivine grains. We observe that the $npFe^0$ volume density has a major effect on the spectrum at visible wavelengths.

4. Conclusions

We have developed a novel numerical approach to compute scattering characteristics of space-weathered planetary bodies. Our method applies more rigorous an algorithm to treat the contributions of the $npFe^0$ particles compared to the standard methods. We have observed that the size and volume fraction of the $npFe^0$ particles have a significant effect on the light-scattering features of an asteroid. Hence our numerical method may allow for a quantitative interpretation of the spectroscopic observations of space-weathered asteroids.

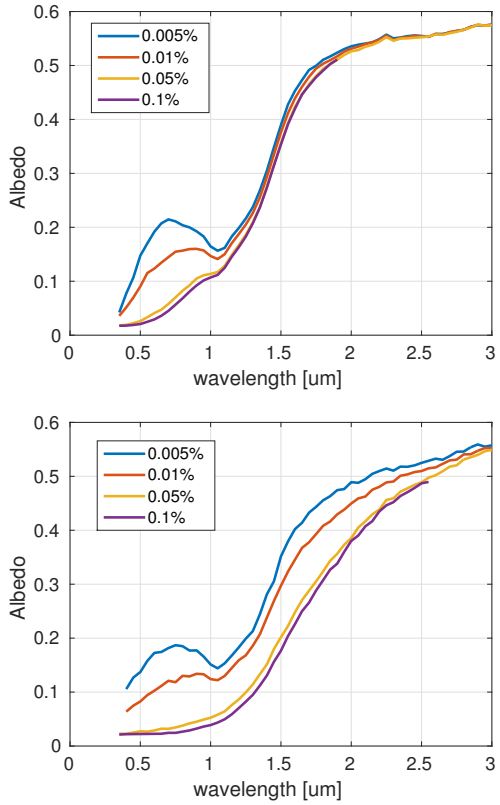

Figure 1: Computed spectra using our model with varying packing densities. The mean radius of npFe^0 particles are 10 nm (top) and 20 nm (top) with the standard deviations of 5 nm (top) and 10 nm (bottom).

Acknowledgements

The research has been funded by the ERC Advanced Grant No 320773 entitled "Scattering and Absorption of ElectroMagnetic waves in ParticuLate media" (SAEMPL).

References

[1] Hapke B. Space weathering from Mercury to the asteroid belt, *J. Geophys. Res.*, 106(E5), 2001.

[2] Carle M. Pieters, and Sarah K. Noble, Space weathering on airless bodies, *J. Geophys. Res. Planets*, 121, 1865–1884, 2016.

[3] Johannes Markkanen, and Alex, J. Yuffa: Fast superposition T-matrix solution for clusters with arbitrarily-shaped constituent particles, *J. Quant. Spectr. Rad. Trans.*, Vol. 189, pp. 181-188, 2017.

[4] Zurk L. Scattering properties of dense media from Monte Carlo simulations with application to active remote sensing of snow, *Radio Science* 31(4), 1996.

[5] Karri Muinonen, Johannes Markkanen, Antti Penttilä, Timo Väisänen, and Jouni Peltoniemi, Multiple scattering by dense random media: Numerical solution, *2016 URSI International Symposium on Electromagnetic Theory (EMTS)*, Espoo, pp. 400-403, 2016.

EPSC Abstracts
Vol. 11, EPSC2017-849, 2017
European Planetary Science Congress 2017

3D radiative transfer code for polarized scattered light with aligned grains

V.-M. Pelkonen (1), A. Penttilä (1), M. Juvela (1), and K. Muinonen (1,2)
(1) Department of Physics, University of Helsinki, Helsinki, Finland (veli-matti.pelkonen@helsinki.fi), (2) Finnish Geospatial Research Institute FGI, Masala, Finland

Abstract

We are working on a 3D Monte Carlo radiative transfer code which incorporates hierarchical grid structure (*octree*) and the full Stokes vector for both the incoming radiation and the radiation scattered by dust grains. The dust model can include different populations of dust, differing in composition, size distribution, shapes, and orientation. The non-spherical dust grains can be randomly aligned, or a fraction of them can be aligned with the magnetic fields (in particular, by the radiation field via radiative torques, RATs). The code will be a valuable tool in studying polarized scattered light from cometary comae in the solar system and from protoplanetary disks in the exoplanetary context.

1. Introduction

Polarized scattered light has been observed in cometary comae [1] and in circumstellar disks [9]. An example of a cometary coma is given in Figure 1. Polarized scattered light carries information about the grains from which the light scattered. However, modelling polarized scattered light is a complicated problem. So far, most scattering codes consider either optically thin cases, where radiative transfer is not necessary, or only do one-dimensional (1D) radiative transfer. Three-dimensional (3D) radiative transfer is mainly focused on unpolarized radiation, which is easier to calculate.

We are in the process of developing a 3D radiative transfer code, which will calculate the full Stokes vector of the scattered light, not just the intensity. In addition, we will be able to have grains aligned in the magnetic field, and calculate their effect on the arising polarization of the scattered light.

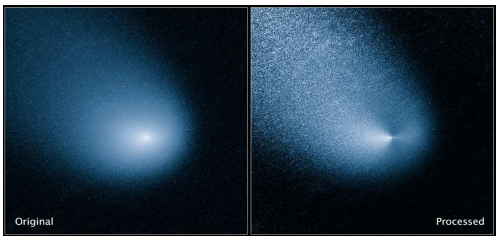

Figure 1: Comet C/2013 A1 coma captured by Wide Field Camera 3 on Nasa's Hubble Space Telescope. Processed image (right) shows jets coming from the comet's nucleus, which is too small to be seen in the images. The coma is about 20000 km across.[7]

2. Radiative transfer code

2.1 CRT code

The radiative transfer code is based on the CRT code [6][5], which was originally developed to study continuum dust emission from interstellar clouds. However, in order to do so, the radiation field impinging on the dust grains within the optically thick cloud has to be solved. While the code allows for internal sources as well, usually the radiation source is outside.

The 3D model cloud is divided into cubic cells, each with constant density. The optical depths for absorption and scattering, as well as the parameters of the scattering function are calculated for each cell. The Henyey-Greenstein formula [2] and the asymmetry parameter g are used to define the scattering function. The radiation field is calculated with Monte Carlo methods. Model rays are initiated at random locations at the cloud boundary in order to simulate the background radiation, and within the cloud to simulate emission from the dust and possible internal sources. The path of the model ray is traced in the cloud. A model ray represents a number of real rays. Absorbed

intensity is counted in each cell that is crossed, and from time to time, the model ray is scattered towards a new direction as determined by the dust model. Because of the frequency dependence of the scattering probability, the simulation has to be carried out separately for each frequency.

2.2 The new code

In the code under development, we take the framework provided by the CRT code, but add the *octree* hierarchical grids, the full Stokes vector rather than just intensity for the model ray, and non-spherical grains which may or may not be aligned with the magnetic field. In *octree* grid format an upper level cell can be divided into 8 subcells by halving the cell in each of the three axis. Levels of further refinement of the grid may be added, as shown in Figure 2.

Due to the non-spherical grains and the polarization, the scattering problem will be the main issue for the code and most time consuming. The scattering parameters will be taken from the models for individual grains. We can introduce populations of different grain shapes into the dust model, and randomly select, based on their amounts, from which shape the model ray scatters. Similarly, we can include aligned and non-aligned subpopulations of these grains, based on the grain alignment calculations (such as using RATs[4][3]), to see which grains should be oriented with the magnetic field, or, in the absence of a magnetic field close to the comet nucleus, with another axis of alignment (e.g., the radiation direction[4]). The 3D nature of the grid allows us to assign these values for each computational cell, to model phenomena like e.g., cometary jets, such as seen in Figure 1.

The code will record polarized scattered light towards the observer, and it is possible to add multiple observer directions to calculate scattering at different phase angles within a single simulation run. These results can then be compared with the observations of comets, or, in the case of other star systems, of circumstellar disks, to help us study these objects.

Acknowledgements

VMP, AP, and KM acknowledge the financial support from the European Research Council, Advanced Grant No. 320773 entitled Scattering and Absorption of Electromagnetic Waves in Particulate Media (SAEMPL). VMP and MJ acknowledge the support of the Academy of Finland Grant No. 285769.

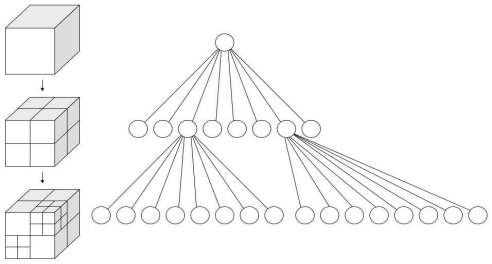

Figure 2: Subdivision of the calculation cube into octants, and the resulting *octree* structure.[8]

References

[1] Hadamcik, E., Levasseur-Regourd, A.C., Hines, D.C., Sen, A.K., Lasue, J., and Renard, J.-B.: Properties of dust particles in comets from photometric and polarimetric observations of 67P, MNRAS, Vo. 462, pp. 507-515, 2016.

[2] Henyey, L.G. and Greenstein, J.L.: Diffuse radiation in the Galaxy, ApJ, Vol. 93, pp. 70-83, 1941.

[3] Herranen, J., Markkanen, J., and Muinonen, K.: Dynamics of interstellar dust particles in electromagnetic radiation fields, Radio Science, submitted.

[4] Hoang, T., Lazarian, A.: Grain alignment by radiative torques in special conditions and implications, MNRAS, Vol. 438, pp. 680-703, 2014.

[5] Juvela, M.: Efficient Monte Carlo methods for continuum radiative transfer, A&A, Vol. 440, pp. 531-546, 2005.

[6] Juvela, M. and Padoan, P.: Dust emission from inhomogeneous interstellar clouds: Radiative transfer in 3D with transiently heated particles, A&A, Vol. 397, pp. 201-212, 2003.

[7] NASA, ESA, and J.-Y. Li (Planetary Science Institute) - https://www.nasa.gov/press/2014/march/nasas-hubble-space-telescope-spots-mars-bound-comet-sprout-multiple-jets/

[8] WhiteTimberwolf, PNG version: Nü - Own work, CC BY-SA 3.0, https://commons.wikimedia.org/w/index.php?curid=9851485

[9] Wolff, S.G., Perrin, M., Millar-Blanchaer, M.A. et al.: The PDS 66 circumstellar disk as seen in polarized light with the Gemini Planet Imager, arXiv:1601.07248

EPSC Abstracts
Vol. 11, EPSC2017-887-1, 2017
European Planetary Science Congress 2017

UV-Vis-NIR spectral modeling of meteorites using novel multiple-scattering methods

J. Martikainen (1), A. Penttilä (1), M. Gritsevich (1), and K. Muinonen (1,2)
(1) Department of Physics, P.O. Box 64, FI-00014 University of Helsinki, Finland, (2) Finnish Geospatial Research Institute FGI, P.O. Box 84, FI-00521 Helsinki, Finland (julia.martikainen@helsinki.fi)

Abstract

We have measured the reflectance spectra of the Osceola meteorite, three lithologies of the Chelyabinsk meteorite (light-colored, dark-colored, and impact melt), and 30 different centimeter-sized meteorite pieces with the University of Helsinki UV-Vis-NIR integrating-sphere spectrometer. Spectral modeling for the meteorite pieces has been carried out by utilizing the SIRIS light-scattering code.

1. Introduction

Asteroids provide us information on the evolution of the Solar System. Meteorites and asteroids can be linked by matching their respective reflectance spectra. However, this is difficult because the spectral features depend strongly on the surface properties, and the surfaces of the meteorites are free of regolith dust present in the asteroids. To better interpret the spectra, we need to understand the surface differences better, for example whether the material is fresh or weathered, and gain more knowledge of the light-scattering physics involved.

2. Samples and Measurements

We have utilized the University of Helsinki UV-Vis-NIR (0.25-3.2 microns) integrating-sphere spectrometer to measure the reflectance spectra of the Osceola meteorite, three lithologies of the Chelyabinsk meteorite (light-colored, dark-colored, and impact melt)[1], and 30 centimeter-sized meteorite pieces borrowed from the mineral cabinet of the Finnish Museum of Natural History. 23 of these samples are ordinary chondrites, four are HED meteorites, one is an aubrite and one is an enstatite. The spectral measurements were carried out using a wavelength range of 250 to 2500 nm with 5-nm sampling steps.

Figure 1: Four measured meteorite samples.

3. Spectral modeling

The reflectance spectra of meteorites can be modeled by combining the most common materials that dominate their spectral features, such as olivine, pyroxene, and iron. We utilize a new code that is based on SIRIS light-scattering code, which simulates light by Gaussian-random-sphere particles large compared to the wavelength of the incident light[2]. The new version models correctly the inhomogeneous nature of the wave due to the absorption in the media. For the computations, we need the complex refractive indices of the materials as input parameters. The refractive indices for olivine and iron are derived from [3], [4], and [5] (data retrieved from Jena Database for Optical Constants for Cosmic Dust and Refractiveindex.info, and further processed by A. Penttilä). The refractive indices for pyroxene were obtained by utilizing an optimization code that utilizes SIRIS-code and the measured reflectance spectrum of the material.

4. Summary and Conclusions

The modeled reflectance spectra for four meteorite samples are shown in Figure 2, and the materials used in the models are shown in Table 1. The small dif-

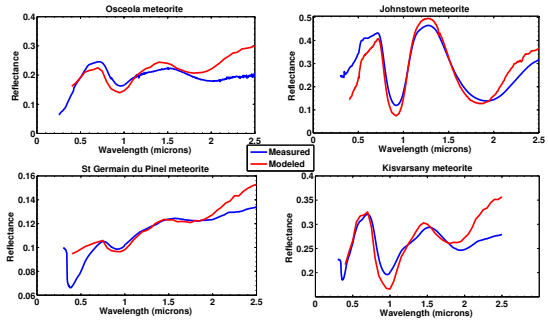

Figure 2: Measured and modeled reflectance spectra.

ferences between the measured and modeled spectra can be caused by a) small amounts of other materials than olivine, pyroxene and iron in the meteorite, b) slightly different type of olivine or pyroxene that was used in the model, and c) the presence of nanoiron in the media, which would explain the difference above 2 micrometers.

Meteorite	**Materials used in the model**
Osceola	55% olivine, 45% pyroxene, 1% microiron
Johnstown	Pure pyroxene (bronzite)
St Germain du Pinel	55% olivine, 45% pyroxene, 4% microiron
Kisvarsany	65% olivine, 35% pyroxene, 0.1% microiron

Table 1: The materials used in the models.

Acknowledgements

The research is funded by the ERC Advanced Grant No. 320773 (SAEMPL).

References

[1] Kohout T. et al. (2014) Icarus, 228, 78–85

[2] K. Muinonen et al. (2009), JQSRT 110, 1628-1639

[3] D. Fabian et al., Astron. Astrophys. 378, 228

[4] P. B. Johnson and R. W. Christy (1974), Phys. Rev. B 9, 5056-5070

[5] M. A. Ordal et al. (1998), Appl. Opt. 27, 1203-1209.

EPSC Abstracts
Vol. 11, EPSC2017-978, 2017
European Planetary Science Congress 2017

Transition of light-scattering properties of complex medium as the medium volume increases

G. Videen (1,2), T. Väisänen (3), J. Markkanen (3), A. Penttilä (3) and K. Muinonen (3,4)
(1) Army Research Lab, Adelphi, Maryland, USA, (2) Space Science Institute, Boulder, USA, (3) Department of Physics, University of Helsinki, Helsinki, Finland, (4) Finnish Geodetic Institute, Masala, Finland (gorden.w.videen.civ@mail.mil)

Abstract

We develop a radiative-transfer coherent-back-scattering (RT–CB) model that provides the possibility of calculating light-scattering properties from a dense medium composed of arbitrary particles. We use this algorithm to investigate the transition of the light-scattering curves from what would traditionally be considered to be single particles to that of extended media. What results is not a monotonic change in the light-scattering properties. For many of the light-scattering properties, we see a change to some maximum value occurring at approximate size parameters $kR \sim 100$. Then the properties tend to decrease, often to approximately half this original value.

1. Introduction

Over the past few decades, significant progress has been made in producing algorithms capable of calculating light-scattering properties of single particles. The Discrete Dipole Approximation (DDA) [1]-[3] and the Finite-Difference Time-Domain (FDTD) techniques [4]-[6] are each capable of calculating the light scattered by arbitrarily shaped particles. Unfortunately, the number of calculations, and resulting computation time, greatly increase with particle size, making calculations of extended media a pipedream. To consider such media, radiative-transfer techniques have been employed. We recently have developed a method that incorporates coherent backscattering that is efficient at calculating the light scattering from dense media [7] and have verified its results with those of exact calculations of a medium composed of spheres [8].

2. Results

In Figure 1, we present sample calculations of various light-scattering properties of a spherical volume containing spheres as a function of phase angle α. As the volume increases, we can see the curves evolve toward the bold line (kR = 3000), which is representative of a large particle.

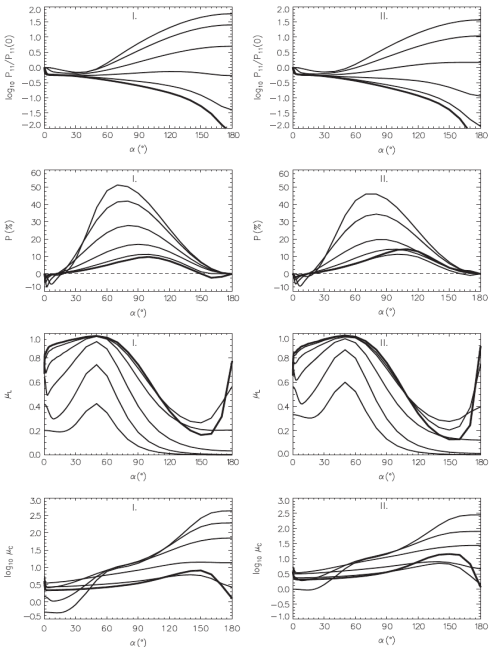

Figure 1: Light scattering by a spherical volume of particulate medium with a size parameter kR = 10, 30, 100, 300, 1000, 3000 (kR = 3000 is shown bold) populated with spherical particles of size kr = 1.76 and refractive index m = 1.50. The first column is for agglomerates having densities ν = 3% (I) and the second is for ν = 6% (II). The separate rows show, from top to bottom, the phase-function intensity, degree of linear polarization, linear polarization ratio, and circular polarization ratio.

Figure 2 shows light-scattering properties as a function of the volume of the medium on a semi-log plot. Note that these properties do not change linearly or even monotonically. Some properties, like the minimum of polarization, and the linear and circular polarization rations in panels 2a, 2e, and 2f, respectively have maxima/minima at approximately $kR \sim 100$.

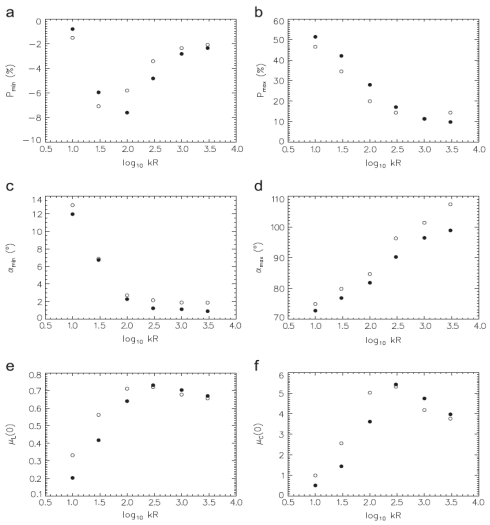

Figure 2: Plots of various scattering parameters as a function of agglomerate size *kR*. Plots show magnitudes of (a) P_{min}, (b) P_{max}, phase angle positions of (c) P_{min}, (d) P_{max}, (e) linear polarization ratio μ_L and (f) circular polarization ratio μ_C at $\alpha = 0^o$. Closed circles are for $\nu = 3.0\%$, and open circles are for $\nu = 6.0\%$.

3. Conclusion

We have used the RT-CB method to examine the transition of light-scattering characteristics of a volume of scatterers as the volume increases. We see that for many properties, there is not a monotonic increase as the final value is reached asymptotically. We have made calculations at different densities and do see differences in this transition value as the density changes. At present, we are making calculations of material having much greater densities than are shown here.

References

[1] Purcell EM, Pennypacker CR. Scattering and absorption of light by nonspherical dielectric grains. Astrophys J 1973; 186:705–14.

[2] Penttilä A, Zubko E, Lumme K, Muinonen K, Yurkin MA, Draine B, et al. Comparison between discrete dipole implementations and exact techniques. J Quant Spectrosc Radiat Transf 2007; 106:417–36.

[3] Zubko E, Petrov D, Grynko Y, Shkuratov Y, Okamoto H, Muinonen K, et al. Validity criteria of the discrete dipole approximation. Appl Opt 2010; 49:1267–79.

[4] Yee KS. Numerical solution of initial boundary value problems involving Maxwell's equations in isotropic media. IEEE Trans Antennas Propagat 1966; 14:302.

[5] Sun W,Fu Q, Chen Z. Finite-difference time-domain solution of light scattering by dielectric particles with a perfectly matched layer absorbing boundary condition. Appl Opt 1999; 38:3141–51.

[6] Sun WB, Videen G, Fu Q, Hu YX. Scattered-field FDTD and PSTD algorithms with CPML absorbing boundary conditions for light scattering by aerosols. J Quant Spectrosc Radiat Transf 2013; 131:166–74.

[7] Muinonen K, Videen G. A Phenomenological single scatterer for studies of complex particulate media. J Quant Spectrosc Radiat Transf 2012; 113:2385.

[8] Muinonen K, Mishchenko MI, Dlugach JM, Zubko E, Penttila A, Videen G. Coherent backscattering verified numerically for a finite volume of spherical particles. Astrophys J 2012; 760:118.

[9] Videen G, Muinonen K, Light-scattering evolution from particles to regolith. J Quant Spectrosc Radiat Transf 2015; 150:87–94.

EPSC Abstracts
Vol. 11, EPSC2017-993, 2017
European Planetary Science Congress 2017

Experimental light scattering by ultrasonically controlled small particles — Implications for Planetary Science

M. Gritsevich (1,2), A. Penttilä (1), G. Maconi (1), I. Kassamakov (1), J. Markkanen (1), J. Martikainen (1), T. Väisänen (1), P. Helander (1), T. Puranen (1), A. Salmi (1), E. Hæggström (1) and K. Muinonen (1,3)

(1) Department of Physics, University of Helsinki, Finland, (maria.gritsevich@helsinki.fi), (2) Institute of Physics and Technology, Ural Federal University, Ekaterinburg, Russia, (3) Finnish Geospatial Research Institute FGI, Masala, Finland.

Abstract

We present the results obtained with our newly developed 3D scatterometer — a setup for precise multi-angular measurements of light scattered by mm- to µm-sized samples held in place by sound. These measurements are cross-validated against the modeled light-scattering characteristics of the sample, i.e., the intensity and the degree of linear polarization of the reflected light, calculated with state-of-the-art electromagnetic techniques.

We demonstrate a unique non-destructive approach to derive the optical properties of small grain samples which facilitates research on highly valuable planetary materials, such as samples returned from space missions or rare meteorites.

1. Introduction

Electromagnetic scattering is a fundamental physical process that allows inferring characteristics of an object studied remotely. This possibility is enhanced by obtaining the light-scattering response at multiple wavelengths and viewing geometries, i.e., by considering a wider range of the phase angle (the angle between the incident light and the light reflected from the object) in the experiment.

Planetary environments represent numerous examples of scattering media composed of particles. There is a fundamental difficulty, however, in bridging the gap between the light-scattering theory and experiment: while existing theoretical models can be used reliably to simulate scattering by a fixed finite object or random particles [1], thorough experimental work has mostly been performed with light scattered from surfaces, see e.g. [2-4].

2. Bridging the gap

Within the ERC Advanced Grant project SAEMPL (http://cordis.europa.eu/project/rcn/107666_en.html) we have assembled an interdisciplinary group of scientists to develop a fully automated, 3D scatterometer that can measure scattered light at different wavelengths from small particulate samples [5, 6]. The setup comprises: (a) a PXI Express platform to synchronously record data from several photomultiplier tubes (PMTs); (b) a motorized rotation stage to precisely control the azimuthal angle of the PMTs around 360°; and (c) a versatile light source, whose wavelength, polarization, intensity, and beam shape can be precisely controlled. An acoustic levitator is used to hold the sample without touching it.

To interpret laboratory measurements, we model the light-scattering characteristics of the sample, i.e., the intensity and the degree of linear polarization, by our novel multiple-scattering methods for dense random media, including SIRIS [7] and R^2T^2 (radiative transfer with reciprocal transactions). The R^2T^2 method solves the ensemble averaged Foldy-Lax equation. For example, a near-field correction is implemented in terms of the incoherent volume element that contains all the scattering diagrams that do not cancel out in the near-zone [8]. The incoherent scattering parameters of the volume elements are solved exactly by the fast superposition T-matrix method [9]. This approach extends the applicability of the radiative transfer technique to dense random media.

3. Scattering characteristics of the Chelyabinsk meteorite

To demonstrate our approach we performed detailed measurements of light scattered by a Chelyabinsk

LL5 chondrite particle, derived from the light-colored lithology sample of the meteorite [10].

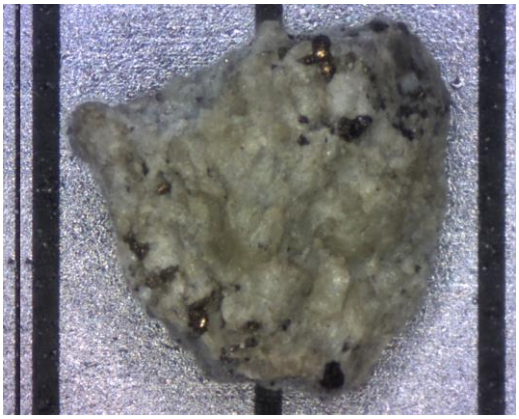

Figure 1: Zoomed-in on particle separated from the light-colored lithology of the Chelyabinsk meteorite. 1-mm scale is given in the background.

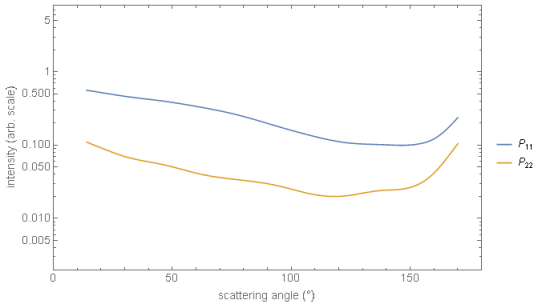

Figure 2: Measured Mueller scattering matrix elements P_{11} and P_{22} for the Chelyabinsk meteorite particle obtained with 530-nm wavelength.

4. Summary and Conclusions

The 3D scatterometer is a valuable tool to measure optical properties of ultrasonically held small particles. The tool can be used to validate theoretical models. It provides unique measurement data to gain new knowledge about the optical properties of both, individual and groups of small particles, including planetary materials.

The device is the first of its kind, since it measures controlled spectral angular scattering including all polarization effects, for an arbitrary object in the µm-cm size scale. It permits a non-destructive, disturbance-free measurement with control of the orientation and location of the scattering object.

Acknowledgements

Funding from the European Research Council under Advanced Grant agreement No. 320773 (SAEMPL).

References

[1] Mishchenko M.I., Travis L.D. and Lacis A.A. 2006: Multiple Scattering of Light by Particles: Radiative Transfer and Coherent Backscattering. Cambridge University Press.

[2] Videen G., Kocifaj M. (Eds.) 2002: Optics of cosmic dust (NATO Science Series), Kluwer Academic Publishers.

[3] Peltoniemi J.I., Gritsevich M., Hakala T., Dagsson-Waldhauserová P., et al. 2015: Soot on snow experiment: bidirectional reflectance factor measurements of contaminated snow. The Cryosphere, 9, 2323–2337.

[4] Zubko N., Gritsevich M., Zubko E., Hakala T., Peltoniemi J.I. 2016: Optical measurements of chemically heterogeneous particulate surfaces. JQSRT 178, 422-431.

[5] Maconi G., Kassamakov I., Penttilä A., Gritsevich M., Hæggström E. and Muinonen K. 2017: Experimental Light Scattering by Small Particles: System Design and Calibration. SPIE conference proceedings, Optical Metrology 2017.

[6] Penttilä A., Maconi G., Kassamakov I., Gritsevich M., Helander P., Puranen T., Hæggström E. and Muinonen K. 2017: Experimental light scattering by small particles: First results with a novel Mueller matrix scatterometer. SPIE conference proceedings, Optical Metrology 2017.

[7] Muinonen K., Nousiainen T., Lindqvist H., Muñoz O., Videen G. 2009: Light scattering by Gaussian particles with internal inclusions and roughened surfaces using ray optics. JQSRT 14-16, 1628–1639.

[8] Muinonen, K., Markkanen, J., Penttilä, A., Väisänen, T., and Peltoniemi, J. (2016). Multiple scattering by dense random media: Numerical solution. In URSI Electromagnetic Theory Symposium EMTS'16, 400-403.

[9] Markkanen J. and Yuffa A.J. 2017: Fast superposition T-matrix solution for clusters with arbitrarily-shaped constituent particles. JQSRT 189, 181-188.

[10] Kohout T., Gritsevich M., Grokhovsky V., Yakovlev G., Haloda J., Halodova P., Michallik R., Penttilä A., Muinonen K. 2014: Mineralogy, reflectance spectra, and physical properties of the Chelyabinsk LL5 chondrite - Insight into shock-induced changes in asteroid regoliths. Icarus, 228, 78-85.

EPSC Abstracts
Vol. 11, EPSC2017-1003, 2017
European Planetary Science Congress 2017

The Mission Accessible Near-Earth Objects Survey (MANOS): Characterizing Small NEOs

C. A. Thomas (1), N. A. Moskovitz (2), A. Thirouin (2), R. P. Binzel (3), E. Christensen (4), F. E. DeMeo (3), M. Hinkle (5, 6), M. J. Person (3), D. Polishook (7), D. E. Trilling (5), M. Willman (8), and B. Burt (2,3)
(1) Planetary Science Institute (1700 East Fort Lowell, Suite 106, Tucson, AZ, 85719, USA, cthomas@psi.edu), (2) Lowell Observatory, (3) Massachusetts Institute of Technology, (4) University of Arizona, (5) Northern Arizona University, (6) University of Central Florida, (7) Weizmann Institute of Science, (8) University of Hawaii

Abstract

The Mission Accessible Near-Earth Object Survey (MANOS) is an ongoing physical characterization survey to build a comprehensive catalog of physical properties. We will use this catalog to investigate the global properties of the small NEO population and identify individual objects that can be targets of interest for future exploration.

1. Introduction

The Mission Accessible Near-Earth Object Survey began in 2013 as a physical characterization survey of newly discovered, sub-km, spacecraft accessible NEOs. We are building a large, uniform catalog of astrometry, photometry, and spectroscopy through queue, remote, and target of opportunity observations.

MANOS has made important progress towards understanding the NEO population. Prior to MANOS, the state of knowledge of NEOs was limited to the largest, kilometer-scale objects.

2. Observations

To accomplish our goals, MANOS uses a wide variety of telescopes (1-8m) in both the northern and southern hemispheres. We focus on targets that have been recently discovered and operate on a regular cadence of queue, remote, target of opportunity observations to enable rapid characterization of small NEOs. Targets for MANOS are selected based on three criteria: mission accessibility, size, and observability. With our resources, we observe 5-10 newly discovered sub-kilometer NEOs per month. The first generation of MANOS has observed ~600 objects since August 2013.

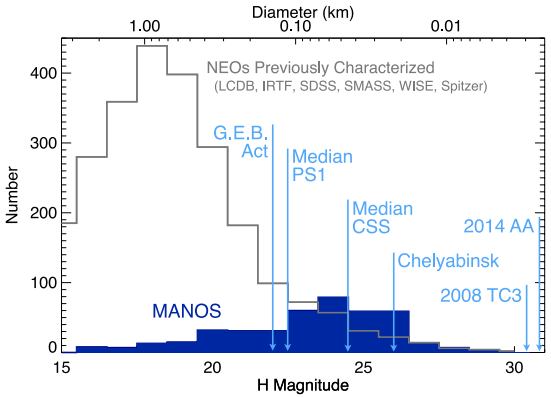

Figure 1: Histogram of NEOs characterized beyond orbit determination (e.g, lightcurves, spectra). The ~600 objects observed by MANOS are included in dark blue. Notable sizes are included in light blue.

3. Photometry

Photometric observations were obtained using Goodman on the Southern Astrophysical Research (SOAR) telescope, the Large Monolithic Imager (LMI) Lowell Observatory's Discovery Channel Telescope (DCT), MOSAIC on the Kitt Peak Mayall 4m, and ANDICAM on the CTIO 1.3m. Initial results from our photometry observations are discussed in Thirouin et al. [1].

MANOS has found 14 sub-km NEOs that are the most suitable candidates for future robotic or human exploration. If we assume that the MANOS results are representative of the sub-km NEO population then we estimate that 10,000 to 1,000,000 NEOs with diameters between 10m and 1km are expected to be viable mission targets.

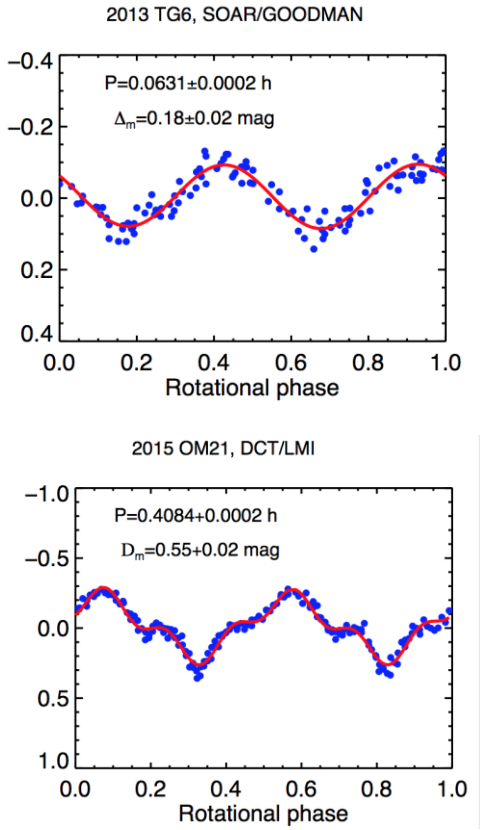

Figure 2: (top) 2013 TG6 (H=26.6) from Goodman on the 4.1m SOAR telescope. (bottom) 2015 OM21 (H=22.4) from LMI on the Discovery Channel Telescope.

4. Spectroscopy

Visible wavelength spectra are obtained using DeVeny on Lowell Observatory's Discovery Channel Telescope (DCT), Goodman on the Southern Astrophysical Research (SOAR) telescope, and GMOS on Gemini North and South. Over 300 NEO spectra have been obtained during our program.

An apparent compositional discrepancy exists between large (>1km) NEOs and the meteorite population [2]. We expected the small NEOs observed by MANOS to be direct precursors to the meteorite fall population and bridge the compositional divide previously observed. However, initial results suggest that small NEOs show a larger discrepancy with the meteorite population than their larger brethren [3].

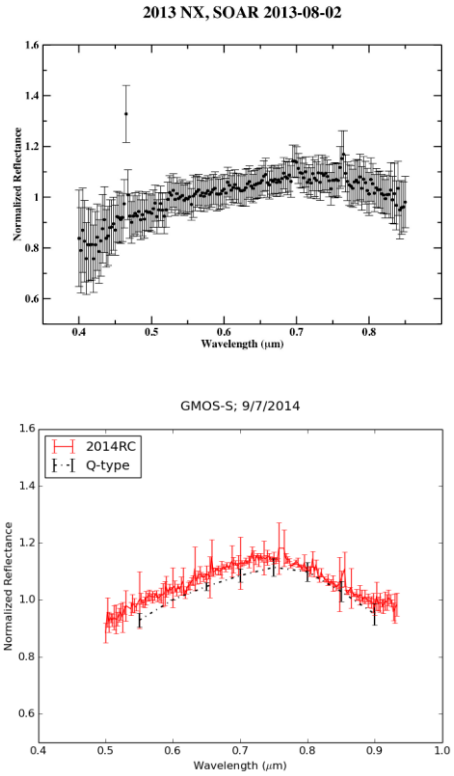

Figure 3: (top) 2013 NX (H=22.0) from the Goodman spectrograph on the 4.1m SOAR telescope. (bottom) 2014 RC (H=26.6, red) from the GMOS spectrograph on the 8.1m Gemini-S telescope.

Acknowledgements

We acknowledge the National Optical Astronomy Observatory (NOAO) and funding support from NASA NEOO grant number NNX14AN82G.

References

[1] Thirouin A. et al. (2016) *AJ*, *152*, 163.

[2] Stuart & Binzel (2004) *Icarus*, *170*, 295-311.

[3] Hinkle (2016) NAU Master's Thesis.